Regional Circulation Characteristics Associated with a Cold Surge Event over East Asia during Winter MONEX

PAO-SHIN CHU[1]

Department of Atmospheric Sciences, Oregon State University, Corvallis, Oregon 97331

SOON-UNG PARK[1]

Department of Meteorology, Seoul National University, Seoul, Korea

(Manuscript received 25 August 1983, in final form 22 February 1984)

ABSTRACT

A case study is presented of the cold surge over East Asia during 9–13 December 1978, using nine vertical levels of Winter MONEX data. The surge event is manifested by a rapid meridional mass flow in the lower troposphere from the midlatitudes (~30°N) to the equator within three days. During the period studied, the lower tropospheric circulation dramatically changed in extent and intensity. With the onset of the surge event, the main divergent maximum began shifting from the South China Sea to southeast China. At the same time, the upper tropospheric circulation correspondingly changed in a reversed order from that of the lower troposphere, and a direct vertical coupling between flows in the low and high troposphere was observed.

The time-averaged meridional mass circulation between 100 and 126°E reveals a two-cell structure; the southern cell is located between the northern South China Sea and the equator, and the northern cell between midlatitudes and the northern South China Sea. Analysis of sensible heat transport indicates that the southern cell is associated with warm air in the south and cold air in the north; thus it resembles a thermally-direct local meridional circulation. Moisture transport analysis shows that the moisture source is found in the southern branch of this cell, and the sink in the northern branch. Conversely, the northern cell is thermally indirect.

The time-mean zonal mass circulation between 32°N and 4°S is marked by two cells, linked by subsidence near the longitudes of the South China Sea. The eastern cell is accompanied by heat and moisture sources while the western cell is associated with heat and moisture sinks.

1. Introduction

During the northern winter, the mean meridional circulation over East Asia is the dominant system in the global atmosphere. It is characterized by ascending warm air over the Indonesian "maritime continent" and descending cold continental air over south China and the adjacent northern South China Sea (Ramage, 1971). One of the most intriguing aspects of this system is a succession of northeasterly cold surges associated with outbursts of the Siberian high over China. Even near the equatorial South China Sea, the effect of a cold surge is felt, being manifested by strengthened northerly or northeasterly winds, although the concomitant temperature signature may not be present due to the rather quick modification of the surge by the underlying warm sea water.

Daily changes in the planetary-scale circulation due to cold surge activity have been studied in detail, based on 200 mb wind data, by Chang and Lau (1980, 1982). They demonstrated that the increase in cold air advection over northern China is responsible for the enhancement of the East Asian local Hadley circulation through increased sinking motion in northern midlatitudes. In response to the surge air, convective activity in low latitudes is enhanced, causing the local Hadley circulation to reach its maximum intensity.

The data collected during the Winter Monsoon Experiment (WMONEX) in 1978–79 have enabled more extensive investigations of winter circulation than ever before. More recently, the interactions between the large-scale (Hadley type) and synoptic-scale (cold surge type) circulations have been investigated through the application of eigenvector analysis to sea-level pressure and surface temperature (Chu and Sikdar, 1983). It is hypothesized that the outburst of cold air in southeast China follows the maximum intensity of the local Hadley circulation by *one or two* days. The cold air advection southward then feeds back to strengthen the meridional overturning *three or four* days later.

During December 1978 there were a few surges and their intensities were weak to moderate (Sadler, 1979). The surge reported on 10 December in Hong Kong is perhaps the most interesting because of its moderate strength. This paper presents an analysis of the structure and time variations of regional circulation accompa-

[1] This work was performed while both authors were affiliated with the University of Wisconsin-Milwaukee, Milwaukee, WI 53201.

nying this surge event, using nine vertical levels (1000–150 mb) of gridded data collected during WMONEX. The period of analysis is 9–13 December.

In its long trajectory southward, the cold surge carries large quantities of mass in the lower troposphere. For this reason, an examination of mass flow in association with propagation of the surge from midlatitudes to the tropics is fundamental to our understanding of the meridional circulation. Since the cold surge is characterized by a cold and dry air mass, it is also of interest to monitor the heat and moisture exchanges accompanying its propagation. Accordingly, the aims of this paper are: 1) to investigate the variations of the kinematic features of the winter troposphere during the surge period; 2) to evaluate quantitatively the mass flow and to depict schematically the mass circulation; and 3) to determine sensible heat and moisture transports in connection with the mass circulation.

2. Data and computational procedures

The University of Wisconsin gridded upper air data set based mainly on FGGE level II-b data over the WMONEX domain is used. This data set contains nine mandatory levels (1000–150 mb), twice per day, covering the period 8–30 December 1978 with a resolution of 2° latitude–longitude. The parameters include east–west (u) and north–south (v) wind components, relative vorticity, horizontal divergence, temperature and moisture, and the domain extends between 36°N–8°S and 96°–130°E (Fig. 1). The editing of level II-b data involves several steps. First, data from each station within the domain are tabulated in time–height format, values beyond physically unreasonable limits being excluded. Second, horizontal fields of wind, temperature and specific humidity are hand-analyzed at each level, again with inconsistent data being deleted. As a final step, FGGE level III-b data are added along the boundaries of the domain. The merged data sets are then gridded using an objective analysis scheme described in Barnes (1973). For details on the editing of this data set, see Mower *et al.* (1983).

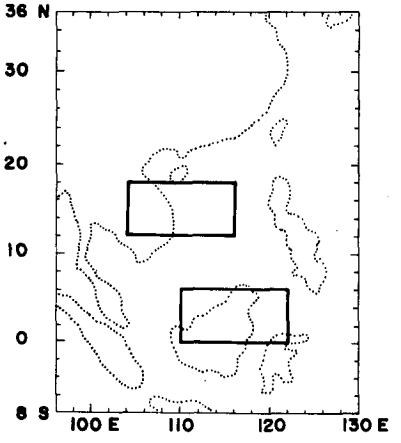

FIG. 1. Map showing the locations of the two areas where the net heat and moisture transports are computed.

Using the Helmholtz theorem, the horizontal wind vector $\mathbf{V}$ can be decomposed into the sum of divergent ($\mathbf{V}_\chi$) and rotational ($\mathbf{V}_\psi$) wind components such that

$$\mathbf{V} = \mathbf{V}_\chi + \mathbf{V}_\psi = \nabla\chi + \mathbf{k} \times \nabla\psi, \tag{1}$$

where χ is the velocity potential, ψ the streamfunction, and $\mathbf{k}$ the unit vector in the vertical direction. These two components are defined separately as

$$\mathbf{k} \cdot \nabla \times \mathbf{V} = \nabla^2\psi, \tag{2}$$

$$\nabla \cdot \mathbf{V} = \nabla^2\chi, \tag{3}$$

where ∇^2 is the Laplacian operator. Using the computed divergence and the vertical component of the vorticity from the data set, Eqs. (2) and (3) are solved for the ψ and χ fields using the direct method of the discrete Poisson equation (Dorr, 1970). We have used mass-adjusted divergence fields such that the vertical mass fluxes at 1000 and 100 mb vanish. Inasmuch as the study domain is regional, an appropriate boundary condition for ψ is required. Boundary values of χ are set to zero and the streamfunction is obtained using the method of version III suggested by Hawkins and Rosenthal (1965). Since the boundary condition for χ is assumed to be zero along the periphery, the following calculations are performed using the entire domain except for the outer two boundaries. It is recognized that this imposed boundary condition may give gradients of the χ-fields somewhat different than those derived from the global domain. This is the inherent shortcoming of the regional-scale domain used in this study.

From Eq. (1), the zonal (u_χ) and meridional (v_χ) components of the divergent wind $\mathbf{V}_\chi$ are, respectively,

$$u_\chi = \partial\chi/\partial x, \quad v_\chi = \partial\chi/\partial y.$$

Thus, the intensity of meridional circulation, I_m, associated with the divergent wind is

$$I_m = \frac{1}{L_x}\int_{X_1}^{X_1+L_x} v_\chi dx, \tag{4}$$

where X_1 is the starting longitude and L_x the length of a zonal extension. The zonal extent of the I_m integral is 100–126°E, and I_m is calculated at six latitudinal bands centered at 29, 24, 18, 12 and 6°N, and the equator. Each band consists of a 10° latitudinal span, except for the extreme northern band where only 8° of latitude are used due to the constraint in our study domain. Likewise, the intensity of zonal circulation, I_z, is

$$I_z = \frac{1}{L_y}\int_{y_1}^{y_1+L_y} u_\chi dy, \tag{5}$$

where y_1 is the starting latitude and L_y the length of a meridional extension. The meridional extent of the

I_z integral is 32°N–4°S, and I_z is calculated at four longitudinal bands centered at 104, 110, 116 and 122°E. Again, the 10° longitudinal bands are used.

With the computed I_m and I_z, we define the vertically-integrated mass flux F of the divergent wind from levels P_1 to P_2 as

$$F_m = \frac{1}{g}\int_{P_1}^{P_2} I_m dp, \tag{6}$$

$$F_z = \frac{1}{g}\int_{P_1}^{P_2} I_z dp, \tag{7}$$

where the subscripts m and z represent the meridional and zonal components, respectively.

In a way similar to the mass flux computation, the vertically-integrated sensible heat (H) and moisture (M) transports associated with the divergent wind are

$$H_m = \frac{1}{g}\int_{P_1}^{P_2} T_m dp, \tag{8}$$

$$H_z = \frac{1}{g}\int_{P_1}^{P_2} T_z dp, \tag{9}$$

$$M_m = \frac{1}{g}\int_{P_1}^{P_2} W_m dp, \tag{10}$$

$$M_z = \frac{1}{g}\int_{P_1}^{P_2} W_z dp, \tag{11}$$

where

$$T_m = \frac{1}{L_x}\int_{X_1}^{X_1+L_x} v_\chi T' dx,$$

$$T_z = \frac{1}{L_y}\int_{y_1}^{y_1+L_y} u_\chi T' dy,$$

$$W_m = \frac{1}{L_x}\int_{X_1}^{X_1+L_x} v_\chi q' dx,$$

$$W_z = \frac{1}{L_y}\int_{y_1}^{y_1+L_y} u_\chi q' dy.$$

Deviations from area mean temperature and mixing ratio are denoted by T' and q', respectively.

3. Mean χ and ψ fields

The time-mean velocity potential fields, $\bar{\chi}$, during the period 9–13 December 1978 at 850, 500 and 200 mb, for the domain bounded by 34°N–6°S, 98–128°E, are presented in Fig. 2. At 850 mb (Fig. 2a), the flow spilling from Indochina to both the equatorial "maritime continent" and northern midlatitudes is apparent. (The flow direction is defined here from negative to positive χ.) A weak east–west circulation is also depicted in Fig. 2a. At 500 mb (Fig. 2b), the pattern is different from that at low levels. The divergent outflow from Celebes toward southeast China and Taiwan is conspicuous. The χ field at 200 mb (Fig. 2c) is approximately inverse to that shown at 850 mb, suggesting a vertically coupled cell. A strong, divergent outflow centered over Borneo at the upper level (Fig. 2c), together with the low-level inflow over the equatorial region (Fig. 2a), indicates a pronounced rising motion over the equator. Conversely, a sinking motion over Indochina is implied by Figs. 2a and c. However, it should be kept in mind that the strongest tropical outflow at 200 mb during WMONEX is observed over the equatorial central Pacific (Sumi and Murakami, 1981; Lau *et al.*, 1983). Thus, the rising motion over Borneo and sinking motion over Indochina do not necessarily imply a connected and closed overturning process. The sinking motion over Indochina contrasts with previous studies in which strong subsidence was observed over central China (Krishnamurti *et al.*, 1973; Murakami and Unninayar, 1977). This difference may result from the short sampling period (five days) of this study versus the long-term observations of previous studies.

Figure 3 shows the time-mean streamfunction $\bar{\psi}$ at 850, 500 and 200 mb. The low-level pattern (Fig. 3a) is marked by the presence of an anticyclonic circulation over south China and a cyclonic circulation (in the

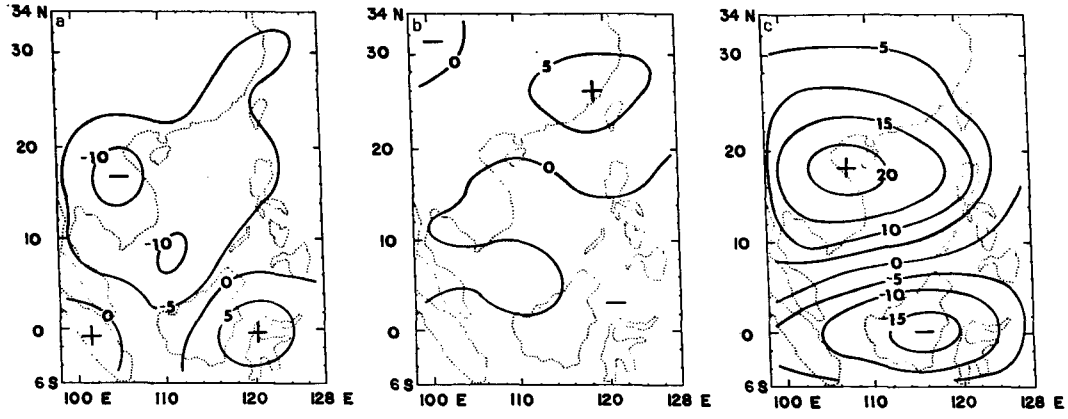

FIG. 2. Time-mean velocity potential (10^6 m^2 s^{-1}) during 9–13 December 1978. Interval is 5 units. (a) 850 mb, (b) 500 mb and (c) 200 mb.

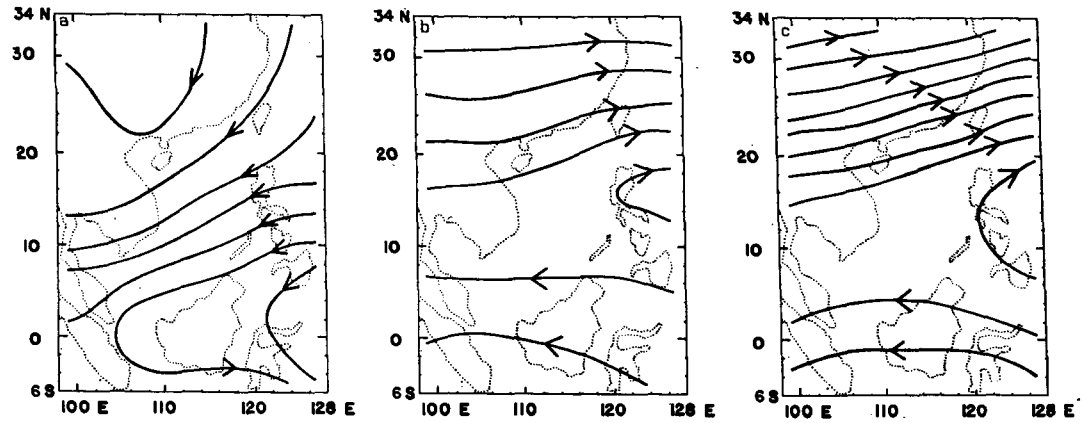

FIG. 3. Mean streamfunction during 9–13 December 1978. (a) 850 mb, (b) 500 mb and (c) 200 mb.

Northern Hemisphere sense) along the equator. The northeasterlies over a large portion of the South China Sea are evident. Streamfunctions at the middle and upper levels (Figs. 3b and c) reveal that midlatitude westerlies are separated from the low-latitude easterlies by the subtropical high pressure which extends out of the analysis domain near 15°N. At 200 mb, a strong north–south streamline gradient is found around 20–30°N, reflecting the existence of the upper-level westerly jet.

4. Temporal variation of χ field

In this section the discussion is focused on the time variations of the χ field at 850 and 200 mb, because flow changes are most prominent at these two levels. At 0000 (all lines GMT) 9 December (Fig. 4a), the most distinct features are that the low-level divergent southerlies and northerlies emanating from the divergent center over the South China Sea move toward central China and Celebes, respectively. Twelve hours later at 1200 9 December, the convergence area indicated by the positive χ maximum in southeast China appears to be located farther eastward and is moderately intensified (Fig. 4b), and the divergence area over the South China Sea tends to be shifted farther inland to Indochina. The convergence area over Celebes also is intensified. At 0000 10 December, in contrast to the preceding day when only one divergent center is observed, two divergence maxima are noted, one in southeast China and the other in the South China Sea (Fig. 4c). The former maximum appears to be related to a cold surge event reported in Hong Kong (Sadler, 1979). The convergence area over southeast China in Fig. 4b is now located over the East China Sea. This eastward displacement coincides with that of the traveling synoptic systems over southeast China documented in Chu and Sikdar (1983). By 1200 10 December (Fig. 4d), the divergent center over southeast China has become established and much of the divergent northerly flow goes into the South China Sea and the equatorial region. It is interesting to note that this pattern is nearly a reversal of that observed on 9 December, except over Celebes where the convergence area remains. This probably indicates the effect of the cold surge on the modulation of regional circulation. On 11 December, the fields are dominated by the divergent center along the southeast China coast (Figs. 4e–f), and the eastward propagation of this center in midlatitudes is still appreciable. By 0000 12 December, the divergent maximum is centered over the South China Sea (Fig. 4g), and the feature becomes similar to that in Fig. 4a. Twelve hours later at 1200 12 December (Fig. 4h), the divergent maximum over the South China Sea has become well developed. Throughout the next 24 hours (Figs. 4i–j) the divergent maximum has diminished considerably while the convergent maximum over the equatorial region has significantly increased, implying the enhancement of ascending motion over the equator.

Figure 5 illustrates the time variations of χ fields at 200 mb. In general, they are approximately reversed from those at 850 mb (Fig. 4). At 0000 9 December, flow is directed from both midlatitudes and the equator toward the South China Sea (Fig. 5a). At 1200 9 December, the upper-level divergent center over southeast China is located further eastward (Fig. 5b), consonant with the displacement of the convergence area at low levels (Fig. 4b). Together with the features presented in Figs. 4a, 4b, 5a and 5b, we note that the lower-level convergence area and upper-level divergent center are coincident, suggesting a vertical coupling which extends deeply throughout the troposphere. In Fig. 5c, the eastward displacement of the divergent maximum in midlatitudes continues to be evident. By 1200 10 December, the most remarkable feature at the upper level is the broadening of the convergence area (Fig. 5d) covering south China and much of Indochina. The divergent maximum over east Borneo and Taiwan has become organized. Throughout the next 72 hours, the upper-level convergent maximum over Hainan and north Vietnam has been maintained (Figs. 5e–j), with

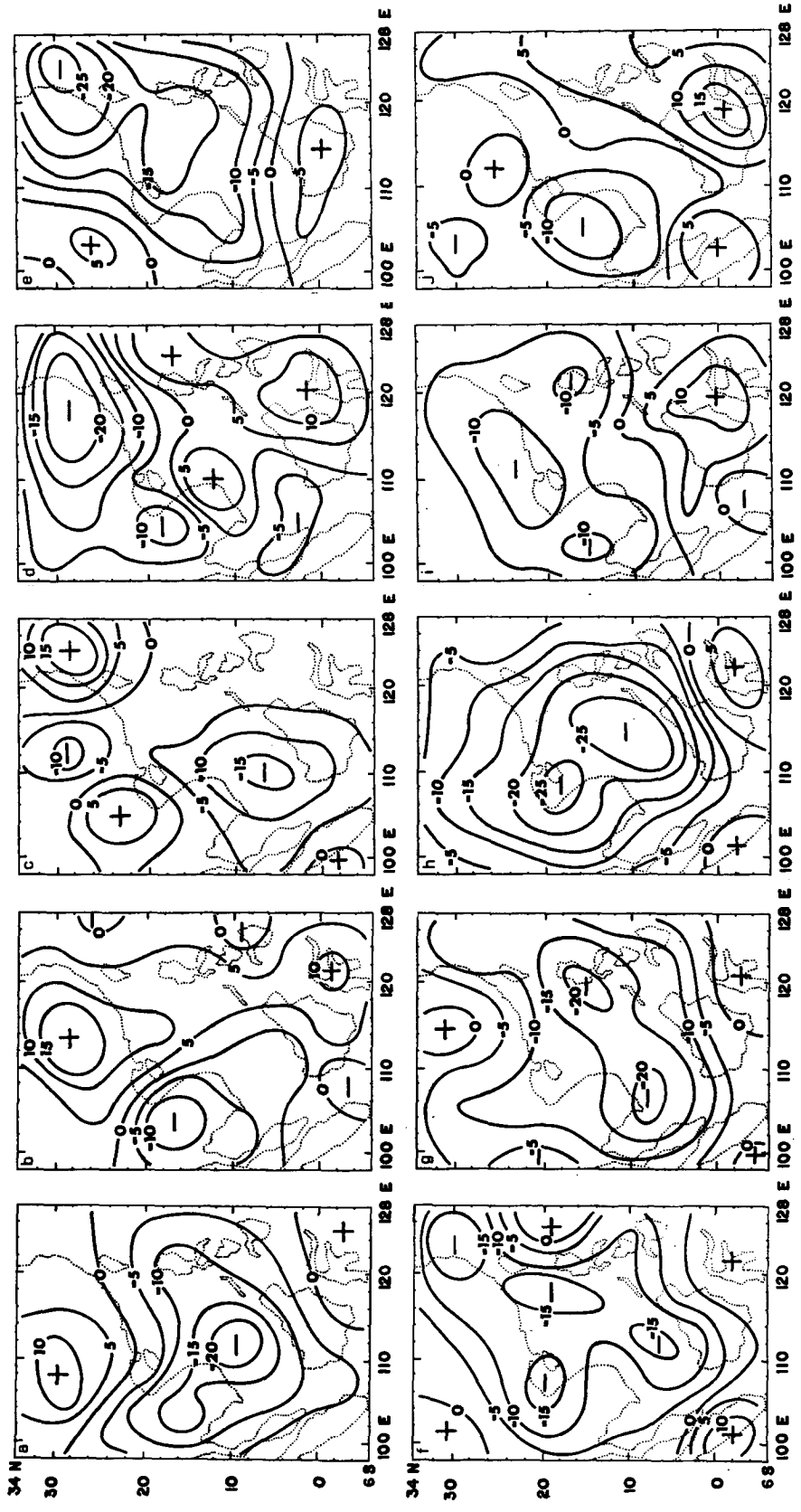

FIG. 4. Velocity potential fields (10^6 m^2 s^{-1}) for intervals in the period 9–13 December 1978 at 850 mb. Two observations per day, at 0000 and 1200 GMT, starting 0000 9 December (a).

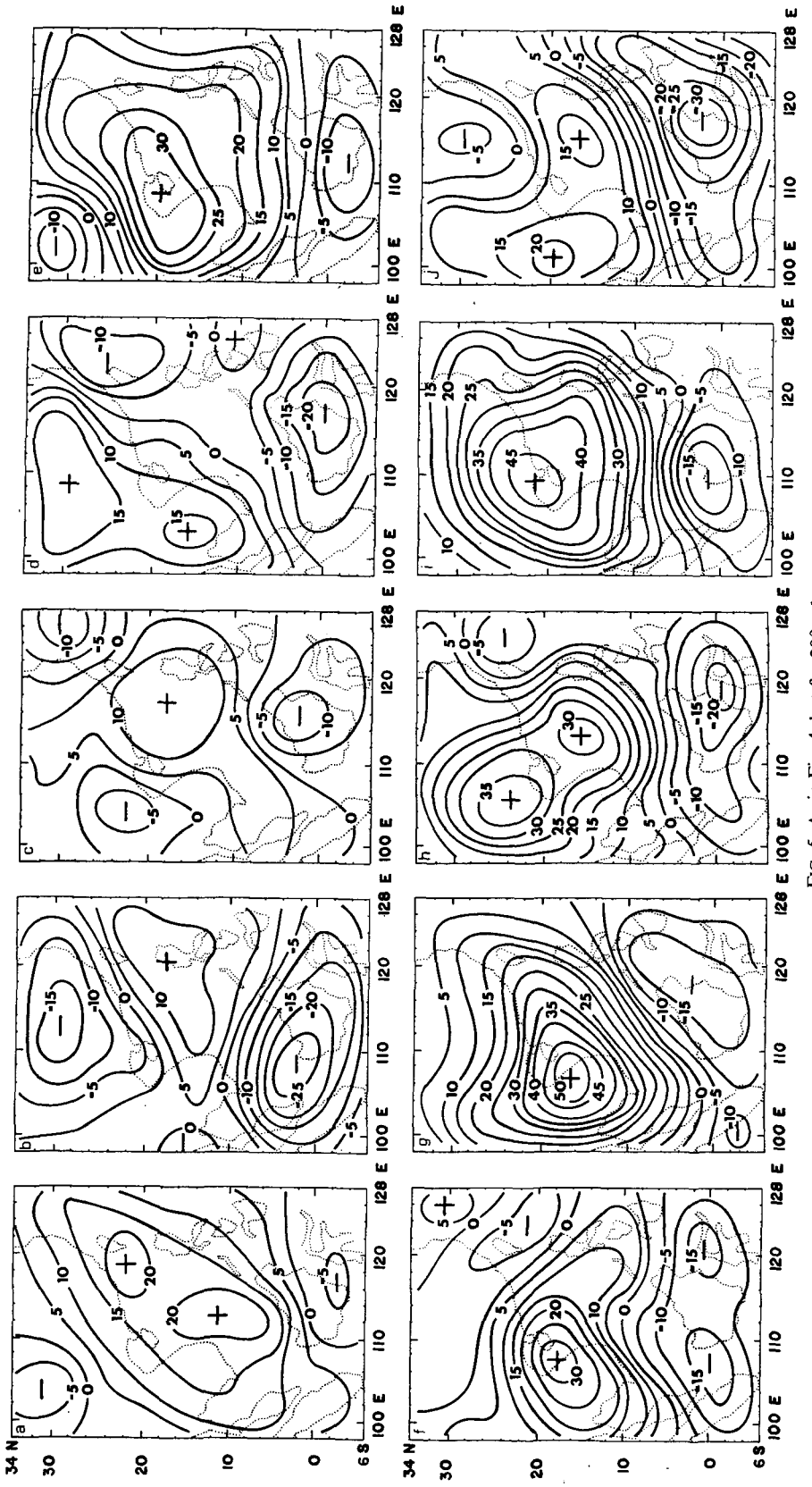

FIG. 5. As in Fig. 4, but for 200 mb.

a maximum intensity at about 0000 12 December (Fig. 5g). The divergent maximum over the equator remains in sight and slowly reaches its maximum intensity at 1200 13 December (Fig. 5j), indicating an enhanced rising motion along the equator.

5. Mass, sensible heat and moisture transports

a. Mass flux

To investigate quantitatively the mass fluxes accompanying the northeasterly cold surge event, the temporal variations of I_m have been plotted at all nine vertical levels during the entire analysis period (not shown). Based on these plots, meridional mass fluxes are integrated vertically at three layers using Eq. (6). The thicknesses of these three layers are somewhat arbitrary. The lower layer is determined from the surface (1000 mb) upward to the level where mass flux changes sign. A typical example is given in Fig. 6. Similarly, the upper layer is determined from the top (150 mb) downward to the level of sign change. The remaining layers are assigned as the middle layer. In general, the lower layer is confined below 700 mb, and the upper layer is somewhere between 150 and 400 mb. Sometimes, due to the deep vertical layers in both the lower and upper troposphere, the middle layer cannot be identified. Even if the middle layer can be discerned, the positive and negative mass flows within that layer tend to offset each other and make the vertically integrated values small. For this reason, the discussion is limited to the lower and upper layers.

Figure 7 illustrates the temporal variations of the vertically-integrated mass flows associated with the meridional component of the divergent wind, F_m, in the lower layer during 9–13 December. The profile indicates that a southward flow is rendered effective by the presence of the cold surge across the entire domain, i.e., starting at 1200 9 December near 30°N and ending at 1200 12 December near the equator. This rapid southward mass flow in the lower layer, accomplished within three days from midlatitudes to the equator, agrees well with the results of Chu and Sikdar (1983). The magnitude of this maximum equatorward flow is $\sim 4.3 \times 10^9$ kg s^{-1} near 30°N and 13×10^9 kg s^{-1} at the equator between 100–126°E. Another noteworthy phenomenon shown by Fig. 7 is that during the entire period the time-averaged mass flow is poleward near 30°N, while equatorward flow prevails over the area south of 18°N. This suggests that mean meridional mass divergence occurs somewhere near the latitudes of the northern South China Sea, which is consistent with the $\bar{\chi}$ analysis presented in Fig. 2.

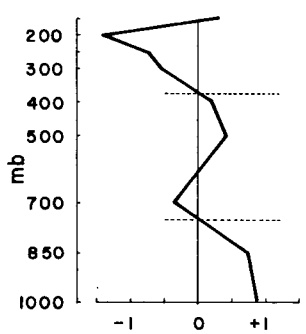

FIG. 6. Vertical profile of meridional mass flow (m s^{-1}) at 1200 GMT 9 December 1978.

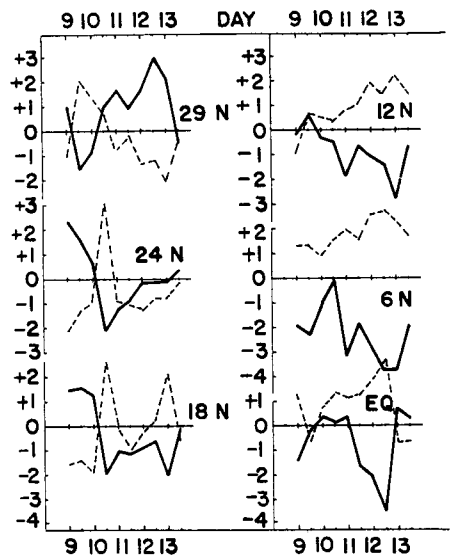

FIG. 7. Vertically-integrated meridional mass flow (10^3 kg m^{-1} s^{-1}) in the lower troposphere (solid line) and upper troposphere (broken line) during 9–13 December 1978.

The vertically-integrated meridional mass flow in the upper layer is also shown in Fig. 7. At 1200 9 December, a strong poleward flux is dominant near 30°N while a strong equatorward flux is observed in the lower level. Concurrent with the establishment of the equatorward mass flow in the lower layer at 1200 10 December, a strong upper-level poleward flux occurs at 24 and 18°N. The time-averaged flux in the upper level indicates that the equatorward mass flow is conspicuous to the north of 18°N while poleward flow is evident in the region south of 12°N.

A synthesis of the mean meridional mass flow in the lower and upper layers (Fig. 7) reveals a vertical circulation consisting of two cells whose descending branch is in the South China Sea and whose ascending branches are in the equatorial region and midlatitudes (Fig. 8a). The position of the descending branch is in agreement with the result of a recent study by Lau *et al.* (1983). Their analysis indicated a convergence of the 200 mb meridional component of the divergent wind over the latitudes of northern Indochina, from the composites of 11 cases of cold surges during the Winter MONEX period. It is noted that the sinking

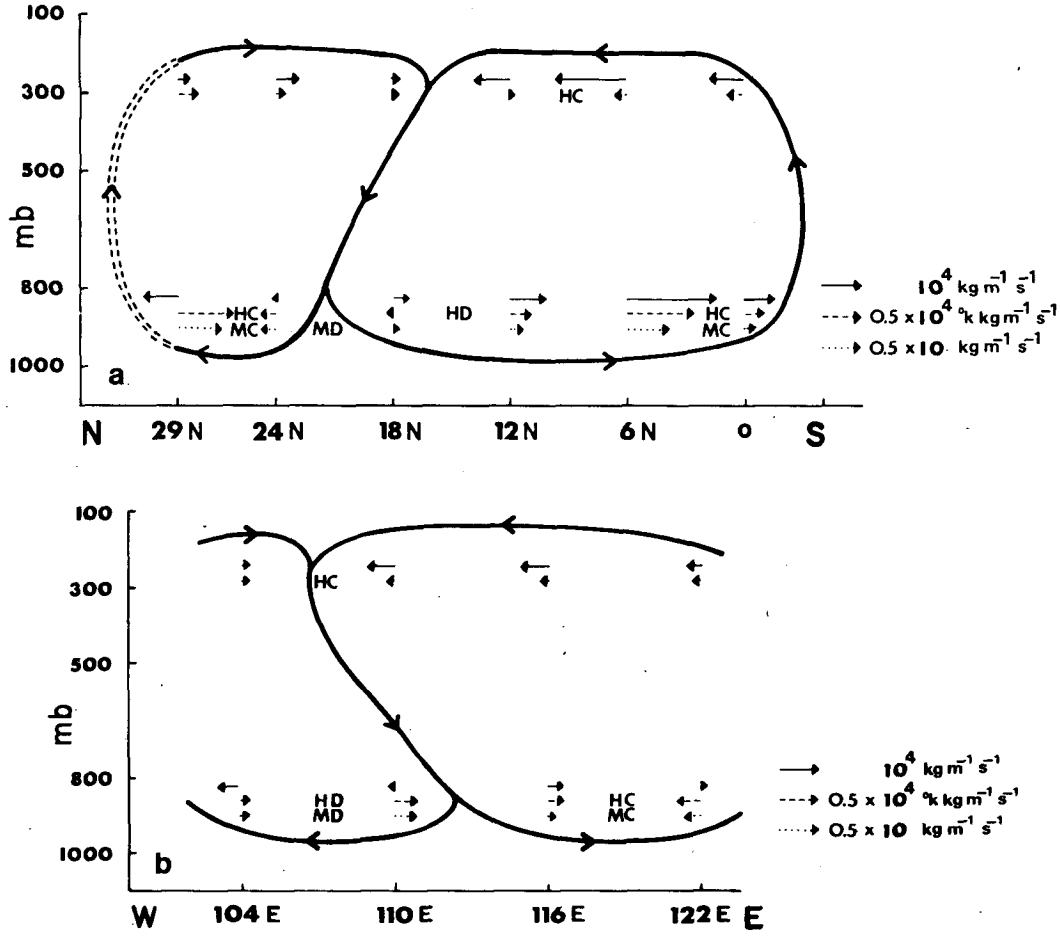

FIG. 8. (a) Schematic diagram showing the time-averaged meridional mass circulation and the accompanying heat and moisture transports. The mass circulation is denoted by solid curves, except near midlatitudes where the double broken line indicates uncertainty in the position of the rising branch. At low levels, mass flow (solid arrow), sensible heat transport (broken arrow), and moisture transport (dotted arrow) are denoted in order. Lengths of arrows are scaled according to their magnitudes. HC and HD denote areas of obvious heat convergence and divergence, respectively. MC and MD are areas of obvious moisture convergence and divergence, respectively. At upper levels, only mass flow and heat transport are shown. (b) As in (a), except for time-averaged zonal mass circulation and the associated heat and moisture transports.

branch in this study tends to tilt slightly equatorward with height. This sinking branch connecting the southern and northern cells reflects the dominance of the subtropical high pressure of the North Pacific, which extends frequently into the South China Sea. The position of this high pressure is depicted clearly in Chang *et al.* (1981) and also in Fig. 3. The upward motion in midlatitudes is inferred from mass continuity due to the equatorward (poleward) flow in the upper (lower) troposphere, together with the downward motion in the northern South China Sea. Another area of strong rising motion is found over the equatorial trough zone where convective activity is expected to be strong.

The vertically-integrated mass flow associated with the zonal component of the divergent wind, F_z, is determined using Eq. (7). Figure 9 shows the temporal variations of F_z in the lower and upper troposphere. In the lower layer, eastward mass flow is observed at 1200 9 December near 104°E, and then it changes to a westward direction until 1200 13 December. Similar variations can also be found in the areas farther eastward to about 116°E. During the entire period the variations of F_z near 122°E tend to fluctuate inversely with those near 104°E. Since the westward and eastward flows predominate in the western and eastern portions, respectively, the time-averaged flow exhibits a low-level mass divergence in the study domain. The variations of the zonal mass flow in the upper layer are approximately inverse to those in the lower layer, and the time-averaged profile would thus be favorable for an upper-level mass convergence.

The mean zonal mass flow exhibits a two-cell structure, i.e., the eastern and western cells are connected by a sinking branch near the longitudes of the South

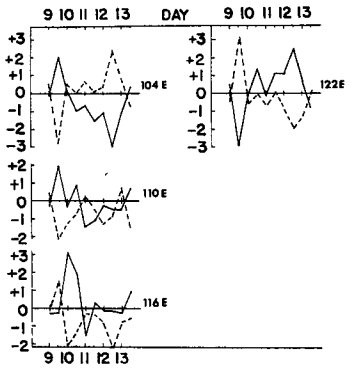

FIG. 9. Vertically-integrated zonal mass flow (10^3 kg m^{-1} s^{-1}) in the lower troposphere (solid line) and upper troposphere (broken line) during 9–13 December 1978.

China Sea (Fig. 8b). The axis of this sinking branch tilts westward with increasing height. Again, this sinking arm may be a result of large-scale subsidence in the subtropical high pressure region. Due to the limited east–west area involved in this study, the rising motion could not be depicted in this analysis. Therefore, the zonal cells should not be interpreted in terms of closed circulation cells.

b. *Sensible heat transport*

In connection with the mass flow, it is of interest to examine the character of heat transport associated with the mass circulation displayed in Fig. 8. The computation for this is carried out for the term $T'\mathbf{V}_x$, not $T'\mathbf{V}'_x$, where the prime denotes the deviation of temperature from the spatial average at any level.

Figure 10, derived from Eq. (8), shows the vertically integrated meridional heat transfer H_m in the lower troposphere. At 1200 9 December, a large positive heat transfer is observed near 30°N. Since the northerly component of the divergent wind ($v_x < 0$) predominates at this time (Fig. 7), a negative temperature deviation ($T' < 0$) resulting from the cold surge is required for the positive heat transport. This positive heat transport can be discerned in an area farther southward to 18°N, where the maximum positive values change successively in space and time. Considering only the meridional heat transport effect at 1200 9 December, the low-level air between 29 and 24°N experiences a temperature decrease of about 3.4°C per day due to the cold air advection. Another noteworthy feature in Fig. 10 is the general prevalence of negative heat transport in the region south of 12°N. Since northerlies prevail in low latitudes (Fig. 7), a positive temperature deviation would account for this negative heat transport. Near the equator, the large heat transport observed between 1200 11 December and 1200 12 December is particularly conspicuous. This is the time when the low-level southward mass flow reaches its maximum (Fig. 7).

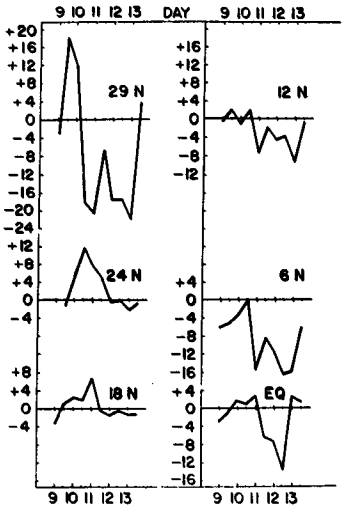

FIG. 10. Vertically-integrated lower-layer meridional sensible heat transport (10^3 K kg s^{-1} m^{-1}) during 9–13 December 1978.

Sensible heat transport in upper levels displays a large negative value from 1200 9 December to 0000 10 December near 30°N (Fig. 11). Since poleward mass flow ($v_x > 0$) prevails (Fig. 7), the negative temperature deviation ($T' < 0$) is thus required for this negative value. This phenomenon, together with the low-level features in Fig. 10, demonstrates that strong cooling, resulting from the surge event, is present in the entire tropospheric column near southeast China. Near the equator, the transport of heat is in general directed poleward, with the strongest transfer occurring between 1200 11 December and 1200 12 December. This positive heat transport is due to the product of the return flow ($v_x > 0$) in the southern cell (Fig. 8a) and the positive temperature deviation. More importantly, a comparison with Figs. 10 and 11 indicates that strong tropospheric warming takes place in low latitudes following the surge event in south China (~30°N), with

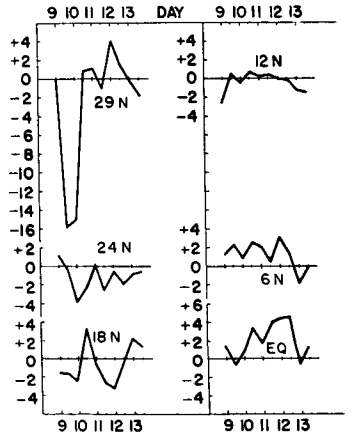

FIG. 11. As in Fig. 10, lower-layer but for the upper troposphere.

a time lag of about two days. This warming has been maintained for 24 hours. It is conceivable that the enhanced ascending motion in the equatorial region, induced by the surge event, would carry considerable heat upward through convection, warming the upper troposphere. Of course, the effect of latent heat release on the warming is not considered in this study but may be important.

The time-mean meridional heat transport H_m in the lower and upper levels is also shown in Fig. 8a. This diagram illustrates a significant low-level heat transport out of the latitudes of the South China Sea (24–6°N), and transport into the latitudinal belts 29–24°N and 6°N–0°. The cooling due to the outward transport of heat in the South China Sea and nearby Indochina may be partly compensated by the adiabatic warming resulting from the subsidence (Fig. 8a). In the upper level, warming occurs over the entire domain, due to the net gain of the heat transport. With respect to the mean meridional mass circulation, the southern cell is characterized by a thermally direct circulation with warm air in low latitudes and cold air near the northern South China Sea. Conversely, the northern cell resembles a thermally-indirect circulation with ascending motion in midlatitudes and descending motion in the northern South China Sea.

The time-averaged zonal heat transport in the lower and upper layer is also presented in Fig. 8b. Low-level net heat loss (cooling) occurs between 104 and 110°E, and a net heat gain (warming) occurs between 116 and 122°E. An upper-level net heat gain (warming) is found between 104 and 110°E, with small variations elsewhere. This is consistent with the mean zonal mass flow in which upper mass convergence is noted in the longitudes of Indochina.

Combining the meridional and zonal heat contributions, it is possible to estimate the magnitudes of the net heat gain or loss in the lower and upper troposphere. For this purpose we selected two areas representative of the Indochina–northern South China Sea region, and the equator (Fig. 1). Our calculation shows that warming prevails more in the lower troposphere, with values of approximately 0.4 K day^{-1} in the equatorial region. In the region representative of Indochina–northern South China Sea, the low-level cooling is ~0.2 K day^{-1}.

c. Moisture transport

It is also interesting to examine the moisture source and sink regions in relation to the mass circulation depicted in Fig. 8. In a way similar to the heat transport, the computation for moisture transfer is performed for the term $q'V_x$. Since the specific humidity is concentrated in the lower portions of the troposphere, only the low-level moisture transport is examined.

Figure 12 shows the vertically-integrated meridional moisture transfer M_m, whose configuration is broadly similar to the heat transport (Fig. 10), although the variations of moisture transport are smaller. Concurrent with the appearance of the cold surge at 1200 9 December in midlatitudes, the meridional moisture transport has positive values, because the northerlies ($v_x < 0$) tend to be dry ($q' < 0$). This positive moisture transport is discerned farther southward to 18°N, as is the case with the heat transport (Fig. 10). In the tropics, the transport by the moist equatorial northerlies is predominantly negative. The large moisture gain during the period 1200 11 December to 1200 12 December is most pronounced; this is about two to three days after the surge occurred in midlatitudes.

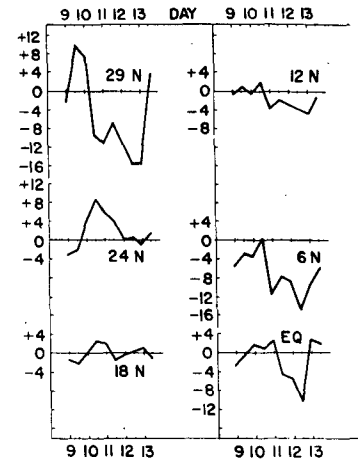

FIG. 12. Vertically-integrated lower-layer meridional moisture transport (kg s^{-1} m^{-1}) during 9–13 December 1978.

The profile of the time-averaged meridional moisture transport (Fig. 8a) implies that the latitudinal distribution of the moisture sink is roughly between 24 and 6°N, while moisture sources are at higher and lower latitudes. This parallels the heat transport profile in which a low-level heat sink is observed in the Indochina–South China Sea region and low-level heat sources are revealed near the equator and in midlatitudes. The time-mean zonal moisture transport (Fig. 8b) indicates that the dominant moisture sink is confined to the longitudes of Indochina, and that the moisture source is found in the longitudes of east Borneo and the Philippines (116–122°E).

For the boxes chosen (Fig. 1), the Indochina–northern South China Sea region shows a moisture loss at a rate of 0.08 g kg^{-1} day^{-1}, while the equatorial region experiences a moisture gain of 0.25 g kg^{-1} day^{-1}.

6. Summary and conclusions

An analysis has been carried out using Winter MONEX data to study the regional circulation over East Asia during the period 9–13 December 1978 when a moderate cold surge occurred. The temporal variations of the regional circulation are discussed in a time sequence of 12-hour intervals. Prior to the occurrence of the surge in midlatitudes, the low-level divergent flow is directed outward from the South China Sea to south China and the equator. When the cold surge occurs along the south China coast, the main low-level

divergent center has shifted to the coast of southeast China and the mass appears to be spilled out from this center toward the equatorial regions. This distribution maintains itself for about a day. After this period, there is a tendency for flow to return to the presurge conditions, with the divergent center located over the South China Sea, and an enhanced low-level convergence in the equatorial region. The corresponding upper-level circulation tends to vary in a reversed order from that of the low-level motion, implying a substantial vertical coupling. However, due to the limited domain used in this study, the rising and sinking air should not be viewed as a simple, closed overturning system.

The cold surge is effective in transporting low-level mass from midlatitudes to the equator within a short time period (~ three days). Temporal variations of temperature and moisture indicate that the surge effect is most pronounced in the region north of 18°N. At the equator, substantial low-level warming and moistening occur two or three days after the surge event in midlatitudes.

The time-averaged meridional mass flow at six latitudinal bands indicates that the regional circulation is dominated by two cells (see Fig. 8a). The southern cell is located between the northern South China Sea and the equator, and the northern cell covers northern midlatitudes and the northern South China Sea. For the southern cell, sensible heat and moisture transport analyses reveal that the heat and water-vapor convergence and divergence occur around the equator and northern South China Sea, respectively. Thus, this cell, with ascending warm, moist air in the south and descending cold, dry air in the north, has the character of a thermally-direct circulation. By contrast, the northern cell is a thermally-indirect circulation.

The time-mean zonal mass circulation also reveals a two-cell structure, connected by subsidence in the longitudes of the South China Sea. The eastern cell is characterized by a heat and moisture source in the lower layers while the west cell is marked by low-level cooling, a moisture sink, and upper-level warming.

In order to estimate quantitatively the net heat (and moisture) gain or loss, one area in the northern South China Sea and another near the equator were selected (see Fig. 1). The northern South China Sea experiences a low-level cooling and drying, and a small upper-level warming. The equatorial region also shows a small upper-level warming, but a low-level warming and moistening.

The two-cell meridional and zonal circulations are linked by a sinking branch, which defines the northern and western boundary of the subtropical high pressure in the North Pacific. This high separates midlatitude westerlies from tropical easterlies. The pulsations of the midlatitude anticyclone in which the cold surge is embedded appear to interact with the subtropical high pressure system. The massive build-up of the midlatitude anticyclone results in the outburst of cold air in southeast China. When this occurs, the subtropical high retreats. The interactions of these two systems are best illustrated in a recent study by Lau *et al.* (1983) from a composite of 11 cases of cold surges over a larger Winter MONEX area. They noted that after a cold surge the 850 mb streamfunction is dominated by two cells, one over East Asia and the other over the eastern North Pacific. The North Pacific cell tends to shift correspondingly eastward when the midlatitude anticyclone over the east China coast moves eastward.

Acknowledgments. We thank Prof. S. Hastenrath and Dr. D. Martin for their comments on this paper, and Dee Dee Bell for typing the manuscript. The comments of Dr. K. Trenberth and anonymous reviewers have helped clarify the presentation. This research was supported by the GARP office of the National Science Foundation under Grant ATS-78-18319. Partial computer support came from the Graduate School, University of Wisconsin-Milwaukee.

REFERENCES

Barnes, S. L., 1973: Mesoscale objective analysis using weighted time-series observations. NOAA Tech. Memo. ERL NSSL-62, National Severe Storms Laboratory, Norman, OK, 60 pp. [NTIS COM-73-10781.]

Chang, C.-P, and K. M. Lau, 1980: Northeasterly cold surges and near-equatorial disturbances over the Winter MONEX area during December 1974. Part II: Planetary-scale aspects. *Mon. Wea. Rev.*, **108**, 298–312.

——, and ——, 1982: Short-term planetary-scale interactions over the tropics and midlatitudes during northern winter. Part I: Contrasts between active and inactive periods. *Mon. Wea. Rev.*, **110**, 933–946.

——, B. K. Cheang and G. T. Chen, 1981: Regional synoptic analysis during phase I of Winter MONEX. Dept. Meteor., Naval Postgraduate School, Monterey, CA, 250 pp.

Chu, P. S., and D. N. Sikdar, 1983: Characteristics of sea level pressure and surface temperature variations during Winter MONEX: December 1978. *J. Meteor. Soc. Japan*, **61**, 717–726.

Dorr, F. W., 1970: The direct solution of the discrete Poisson equation on a rectangle. *SIAM Rev. Pure Appl. Math.*, **12**, 248–263.

Hawkins, H. F., and S. L. Rosenthal, 1965: On the computation of stream functions from the wind field. *Mon. Wea. Rev.*, **93**, 245–252.

Krishnamurti, T. N., M. Kanamitsu, W. J. Koss and J. D. Lee, 1973: Tropical east-west circulations during the northern winter. *J. Atmos. Sci.*, **30**, 780–787.

Lau, K.-M., C.-P. Chang and P. H. Chan, 1983: Short-term planetary-scale interactions over the tropics and midlatitudes. Part II: Winter MONEX period. *Mon. Wea. Rev.*, **111**, 1372–1388.

Mower, R. N., J.-H. Chu, D. W. Martin, B. Auvine and D. N. Sikdar, 1983: Mean state of the troposphere over southeast Asia and the east Indies, December 1978. Dept. Atmos. Sci., University of Wisconsin-Milwaukee, 27 pp.

Murakami, T., and M. S. Unninayar, 1977: Atmospheric circulation during December 1970 through February 1971. *Mon. Wea. Rev.*, **105**, 1024–1038.

Ramage, C. S., 1971: *Monsoon Meteorology*, Academic Press, 296 pp.

Sadler, J. C., 1979: Synoptic scale quick-look for Winter MONEX—December 1978, Dept. Meteor., University of Hawaii, Honolulu, 66 pp.

Sumi, A., and T. Murakami, 1981: Large-scale aspects of the 1978–79 winter circulation over the greater WMONEX region. Part I: Monthly and seasonal mean fields. *J. Meteor. Soc. Japan*, **59**, 625–645.